# Electronic structure of GaAs/AlGaAs quantum double rings in lateral electric field

**Y. Yao[1,2*], T. Ochiai[1], T. Mano[1], T. Kuroda[1], T. Noda[1], N. Koguchi[3], and K. Sakoda[1,2]**

[1] *National Institute for Materials Science, Namiki 1-1, Tsukuba 305-0044, Japan*

[2] *University of Tsukuba, 1-1-1 Tennodai, Tsukuba 305-8577, Japan*

[3] *L-NESS, Universitá di Milano Bicocca, Via Cozzi 52, Milano 20125, Italy*

[*] *E-mail: yao.yuanzhao@nims.go.jp*

Received July 14, 2009

A three-dimensional model of GaAs/AlGaAs quantum double rings in the lateral static electric field is investigated theoretically. The eigenvalue problem with the effective-mass approximation is solved by means of the finite-element method. The energy levels and wave functions of quantum-confined electrons and heavy holes are obtained and show an agreement with our previous theoretical and experimental studies. It is shown in the approximation of neglecting the Coulomb attraction between the electron and heavy hole that a relatively large Stark shift of exciton emission of 4 meV is attainable with an applied electric field of 0.7 kV/cm.

*OCIS codes:* 250.5590, 160.6000, 260.6580.

*doi: 10.3788/COL20090710.0882.*

Recent development of high-quality-factor (high-$Q$) photonic crystal (PC) microcavities[1,2] has made the role of light-emitting quantum nanostructures such as quantum dots (QDs) and quantum rings (QRs) more important than before, since we can achieve unique cavity quantum electrodynamics (QED) experiments by combination of these two components[3−5]. As for the latter, a relatively large Stark shift up to 4 meV was observed for GaAs quantum double rings (QDRs) recently[6], which is a desirable feature for tuning the emission frequency of the nanostructure to the cavity resonance frequency to realize the deterministic Purcell effect[7] for example.

The self-assembled GaAs QDR was fabricated by Mano *et al.*[8] by the droplet epitaxy[9,10] for the first time and its emission spectrum and electronic structure were reported in Refs. [8] and [11]. Because the QDR has a nearly perfect circular symmetry as shown in Fig. 1(a), its electronic state can be characterized by the radial quantum number $N$ and the azimuthal quantum number $l$. Some previous theoretical studies on the QDR used this circular symmetry to simplify the problem[12]. This property was also used for the study of its electronic states in the magnetic field perpendicular to the rings[13−15], which is relevant to the Aharonov-Bohm effect[16].

In the experiment by Yamagiwa *et al.*[6], however, the electric field was applied parallel to the sample surface, so the circular symmetry of the geometry was broken. Thus we have to use another numerical method that does not rely on the circular symmetry to analyze this problem.

In this letter, we report the calculation by the three-dimensional (3D) finite-element method (FEM) without the assumption of the circular symmetry. We show the distribution of the probability density of electrons and heavy holes calculated for the case without an external electric field and their energy shifts induced by the applied electric field.

Although the final goal of our study is the calculation of the Stark-shifted emission spectra of quantum-confined excitons in QDRs, we only report in this letter the energy shift of individual electron and heavy hole confined in the QDR by the 3D FEM with the effective-mass approximation. To obtain the exciton emission spectra, we need to include the Coulomb potential between the electron and hole. For this calculation, we may apply, for example, the method of exact diagonalization of the configuration interaction Hamiltonian, which is somewhat time-consuming and out of the reach of the present letter. So inclusion of the Coulomb potential will be reported elsewhere.

The 3D model of the specimen was directly given by the actual measurement data of the atomic force microscope (AFM) for the GaAs QDR embedded in the $Al_{0.3}Ga_{0.7}As$ barrier layer reported in Ref. [8]. Figure 1(b) shows one half of the vertical cross section of the double ring structure. The GaAs QDR is denoted by gray. The $Al_{0.3}Ga_{0.7}As$ substrate and barrier layer are denoted by white. The amplitude of the wave functions out of the region shown in this figure is assumed to be

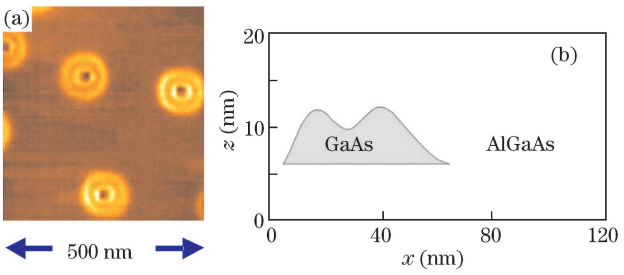


Fig. 1. (a) AFM image of QDRs. (b) One half of the vertical cross section of the double-ring structure of GaAs that is assumed in the calculation. The GaAs QDR is denoted by gray and the $Al_{0.3}Ga_{0.7}As$ substrate and barrier layer are denoted by white. The QDR is circularly symmetric about the $z$ axis. The electric field is assumed to be applied in the positive $x$ direction.

 

**Table 1. Parameters Used in Calculation**

| Quantity | Unit | GaAs | $Al_{0.3}Ga_{0.7}As$ |
|---|---|---|---|
| Electron Effective Mass[17] | $m_0$ | 0.067 | 0.093 |
| Heavy Hole Effective Mass[17] | $m_0$ | 0.51 | 0.57 |
| Conduction Band Offset[18] | meV | 262 | |
| Valence Band Offset[18] | meV | 195 | |

$m_0$ is the genuine electron mass.

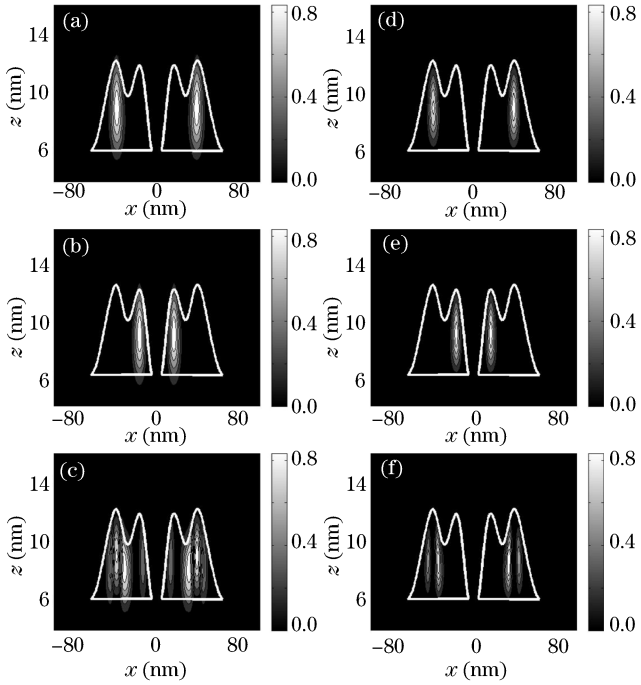


Fig. 2. Distribution of the probability density in the QDR. (a) 1$s$ state, (b) 2$s$ state, and (c) 3$s$ state of the electron and (d) 1$s$ state, (e) 2$s$ state, and (f) 3$s$ state of the heavy hole. The probability density in each panel is normalized by its maximum value.

vanishing, since we are interested in the confined electronic states in the GaAs QDR. The QDR is assumed to be circularly symmetric about the $z$ axis. The electric field is applied in the positive $x$ direction according to the experimental condition.

The conduction band of bulk GaAs has an s-orbital character and is non-degenerate, whereas its valence band has a p-orbital character and is doubly degenerate at the Brillouin zone center. The two bands are called heavy hole and light hole bands. When a nanostructure is formed, this degeneracy is lifted by the structural anisotropy. In the following calculation, we only deal with the heavy hole because the energy levels of the light hole are located out of the relevant frequency range of the present problem.

The effective mass of the electron and heavy hole in the two materials and the band offsets are listed in Table 1, which are the same values used in Ref. [8]. The one-particle Schrödinger equation with the external static electric field was solved by FEM with commercial software, "COMSOL Multiphysics". The discretization mesh size of the finite-element calculation was decreased sufficiently to obtain converged results.

Firstly, we checked the numerical results without the applied electric field. In this case, the configuration has the circular symmetry and all electronic states should be characterized by the principal quantum number $N$ and the azimuthal quantum number (angular momentum) $l$ as mentioned above. We examined the lowest 16 energy levels and their wave functions carefully, and found that the wave functions actually had the expected rotational symmetry and the spectrum of the energy levels was consistent with our previous calculation with the assumption of the circular symmetry[8]. In the following, we denote the $l = 0$, 1, and 2 states by $s$, $p$, and $d$, respectively. We should note that the s states are not degenerate but all other states are doubly degenerate, since there are two independent wave functions proportional to $\exp(il\phi)$ and $\exp(-il\phi)$, respectively, where $\phi$ is the azimuthal angle.

Figure 2 shows the distribution of the probability density on the $xz$ plane (vertical cross section) for the 1$s$, 2$s$, and 3$s$ states of the confined electron and heavy hole where the shape of the QDR is shown by white lines. For both particles, the 1$s$ and 2$s$ states are localized in the outer and inner rings, respectively, which is consistent with our previous calculation[8]. We should note, however, that this feature may not be universal but may depend on the distance between the inner and outer rings and their widths as shown by Climente *et al.*[12]

Now let us proceed to the case of non-zero electric fields. Figure 3 shows the 1$s$ electron energy as a function of the lateral electric field. The origin of the vertical axis is the conduction band bottom of the $Al_{0.3}Ga_{0.7}As$ barrier layer. Black dots denote the numerical results, and solid and dashed lines are linear- and quadratic-fitting curves. The quadratic-fitting curve was obtained from the data with the applied electric field smaller than 0.05 kV/cm as shown in the inset. The transition from the quadratic to linear behavior with increasing amplitude of the electric field is consistent with the degenerate perturbation theory, since we have the 1$p$ state about 0.5 meV above the 1$s$ state.

From Fig. 3, we see that about a 2-meV shift of the 1$s$ state is attained by application of the electric field of about 0.7 kV/cm. Since we have a similar behavior

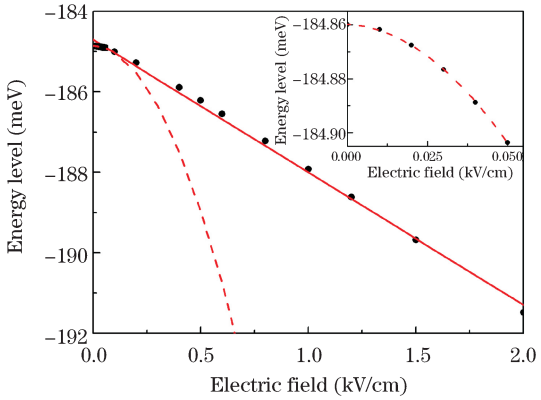


Fig. 3. The 1$s$ electron energy as a function of the lateral electric field. Black dots denote the numerical results. The solid line is a linear-fitting curve, whereas the dashed line is the quadratic-fitting curve for a weak electric field shown in the inset. The origin of the vertical axis is the conduction band bottom of the barrier layer.

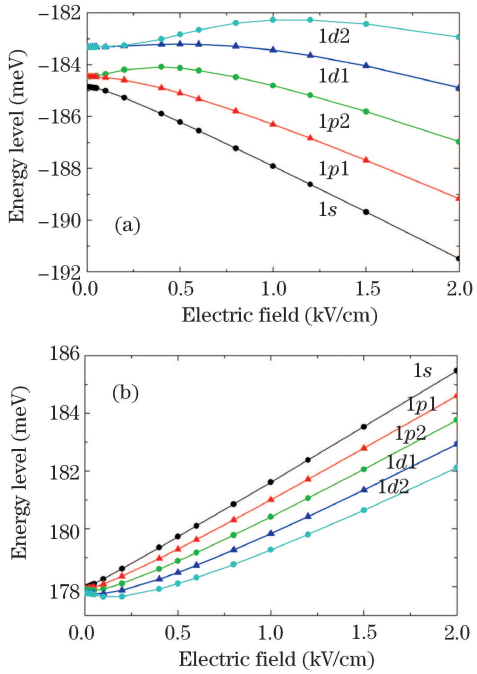


Fig. 4. (a) The lowest five electron states and (b) the highest five heavy hole states as functions of the lateral electric field. Additional numbers 2 and 1 denote states with even and odd parities about the x axis, respectively. The origin of the vertical axis is (a) the conduction band bottom and (b) the valence band top of the barrier layer.

of the 1$s$ heavy hole state as we shall see later, we may conclude that we can expect the 4-meV Stark shift of the GaAs exciton emission found in our recent experiment with an electric field of the order of 0.7 kV/cm.

The energy shifts of 1$s$ to 1$d$ states for the electron and heavy hole are shown in Fig. 4. The origin of the vertical axis of the electron and that of the hole energy are the conduction band bottom and the valence band top of the $Al_{0.3}Ga_{0.7}As$ barrier layer, respectively. As we can see, each degenerate energy level of the 1$p$ and 1$d$ states is split into two by the application of the electric field in the $x$ direction. Their wave functions are symmetric or anti-symmetric about the $x$ axis, since the structure is symmetric about the $x$ axis, the wave functions should have definite parities. The symmetric and anti-symmetric states are denoted by additional numbers 2 and 1, respectively in Fig. 4. In contrast to the case of the 1$s$ electron state shown in Fig. 3, for which all other energy levels are located above it, the energy shift as a function of the applied electric field is not necessarily monotonic for the rest of the energy levels because of the repulsion between levels with the same parity. This feature of our results is consistent with previous calculation for single rings[19].

Another feature of Fig. 4 is the smaller spacing of energy levels for the heavy hole due to its larger effective mass than the electron, which results in the faster transition from the quadratic to linear behavior.

Although we only showed five $N = 1$ states for electron and heavy hole in Fig. 4, we also calculated the energy shifts of the $N = 2$ and 3 states. They showed crossing and anti-crossing of energy levels according to the symmetry of the wave functions when we increased the electric field up to about 1 kV/cm. This feature is also consistent with the symmetry of the geometry and confirms the accuracy of our calculation in which we do not assume particular symmetry of the wave functions *a priori*.

Finally, the transition energy of the exciton ground state, which is attributed to the 1$s$ hole to 1$s$ electron transition, is 1.613 eV and the energy difference to the first excited state, which is attributed to the 2$s$ hole to 2$s$ electron transition, is 9.0 meV in our calculation. These values show a reasonable agreement with our experimental results, that is, 1.68 eV for the former and 8.5 meV for the latter[8], although we do not take the Coulomb interaction into consideration.

In conclusion, energy levels of quantum-confined electrons and holes of $GaAs/Al_{0.3}Ga_{0.7}As$ QDRs in a lateral static electric field were calculated by FEM with the effective-mass approximation. The 3D model assumed in the calculation was directly derived from the actual shape of the specimen measured by AFM. The numerical results showed a smooth and monotonic transition from the quadratic to linear behavior of energy shifts for the 1$s$ electron and 1$s$ heavy hole as a function of the amplitude of the applied electric field, whereas energy levels of other states often showed non-monotonic changes due to the repulsion with adjacent energy levels of the same spatial symmetry. The transition energies of the ground and first excited states of the quantum-confined exciton obtained in the present calculation showed a reasonable agreement with our previous experiment. The electric field necessary to bring about the exciton Stark shift of 4 meV that was recently observed in our experiment was estimated at about 0.7 kV/cm in the approximation of neglecting the Coulomb attraction between the electron and heavy hole.

This work was supported by a Grant-in-Aid for Scientific Research from the Ministry of Education, Science, Sports, and Culture of Japan (No. 20340080).

## References

1. Y. Akahane, T. Asano, B.-S. Song, and S. Noda, Nature **425,** 944 (2003).
2. Y. Akahane, T. Asano, B.-S. Song, and S. Noda, Opt. Express **13,** 1202 (2005).
3. T. Yoshie, A. Scherer, J. Hendrickson, G. Khitrova, H. M. Gibbs, G. Rupper, C. Ell, O. B. Shchkin, and D. G. Deppe, Nature **432,** 200 (2004).
4. K. Hennessy, A. Badolato, M. Winger, D. Gerace, M. Atature, S. Gulde, S. Falt, E. L. Hu, and A. Imamoglu, Nature **445,** 896 (2007).
5. T. Kuroda, N. Ikeda, T. Mano, Y. Sugimoto, T. Ochiai, K. Kuroda, S. Ohkouchi, N. Koguchi, K. Sakoda, and K. Asakawa, Appl. Phys. Lett. **93,** 111103 (2008).
6. M. Yamagiwa, T. Kuroda, T. Mano, K. Sakoda, and N. Koguchi, *in Extended Abstracts of the 68th Autumn Meeting of the Japan Society of Applied Physics* (in Japanese) **3,** 1415 (2007).
7. E. M. Purcell, Phys. Rev. **69,** 681 (1946).
8. T. Mano, T. Kuroda, S. Sanguinetti, T. Ochiai, T. Tateno, J. Kim, T. Noda, M. Kawabe, K. Sakoda, G. Kido, and N. Koguchi, Nano Lett. **5,** 425 (2005).
9. N. Koguchi, S. Takahashi, and T. Chikyow, J. Cryst. Growth **111,** 688 (1991).

10. T. Mano, T. Kuroda, K. Kuroda, and K. Sakoda, J. Nanophoton. **3,** 031605 (2009).
11. T. Kuroda, T. Mano, T. Ochiai, S. Sanguinetti, K. Sakoda, G. Kido, and N. Koguchi, Phys. Rev. B **72,** 205301 (2005).
12. J. I. Climente, J. Planelles, M. Barranco, F. Malet, and M. Pi, Phys. Rev. B **73,** 235327 (2006).
13. J. Planelles and J. I. Climente, Eur. Phys. J. B **48,** 65 (2005).
14. F. J. Culchac, N. Porras-Montenegro, and A. Latge, J. Phys.: Condens. Matter **20,** 285215 (2008).
15. B. Szafran and F. M. Peeters, Phys. Rev. B **72,** 155316 (2005).
16. Y. Aharonov and D. Bohm, Phys. Rev. **115,** 485 (1959).
17. L. Pavesi and M. Guzzi, J. Appl. Phys. **75,** 4779 (1994).
18. M. Yamagiwa, N. Sumita, F. Minami, and N. Koguchi, J. Lumin. **108,** 379 (2004).
19. J. M. Llorens, C. Trallero-Giner, A. Garcia-Cristobal, and A. Cantarero, Phys. Rev. B **64,** 035309 (2001).